Dynamic Normal Mode Initialization for a Limited-area Model

By Takehiko Satomura(*)

Centre National de Recherches Météorologiques/EERM
31057 Toulouse CEDEX, France
(Manuscript received 14 November 1987, in revised form 29 January 1988)

Abstract

The dynamic normal mode initialization scheme (DNI) proposed by Sugi is applied to a limited-area model. Performance of two integration schemes for DNI is examined, and it is shown that Okamura's time integration scheme is inefficient and a backward implicit scheme is appropriate for DNI applied to the limited-area model. All physical processes can be included in the integration cycle of DNI.

Horizontal wind and precipitation rate are compared using a control forecast, a forecast with the nonlinear normal mode initialization (NMI), and with DNI. The deformation of horizontal wind near the mountains is reconstructed by DNI better than by NMI. The area-averaged precipitation is not largely improved by DNI, but the rms error of the precipitation from the control forecast is smaller in DNI than in NMI in the first three hours.

1. Introduction

Limited-area numerical models have been developed to study and to forecast meso-scale weather phenomena since the mid 1970's. The primitive equations are used as the governing equations of the model, and they allow the propagation of gravity waves. In the atmosphere, fast propagating gravity waves typically have small amplitudes compared with the amplitudes of the more slowly propagating synoptic scale weather systems. In numerical atmospheric models, however, large-amplitude high-frequency gravity waves are observed unless special care is taken in specifying the initial conditions. The specification of suitably balanced initial fields is called the initialization.

Three types of the initialization are so far proposed: static initialization, dynamic initialization, and normal mode initialization (NMI)(*1). The NMI method is efficient in eliminating high-frequency gravity waves from the initial field and it is applied to limited-area models (Brière, 1982; Bourke and McGregor, 1983; Craplet, 1985; Bijlsma and Hafkenscheid, 1986) as well as to global or hemispheric models for which NMI was originally formulated. It is well known, however, that NMI has one serious defect: the iterative method used in NMI does not converge if one includes all vertical modes and/or diabatic processes (Williamson and Temperton, 1981; Ballish and Baer, 1985; Rasch, 1985a). Although an underrelaxation method (Kitade, 1983) and a secant approximation method (Rasch, 1985b) were proposed to improve this defect, they could not achieve complete success as pointed out by Rasch

(*) Permanent affiliation: Meteorological Research Institute, Nagamine, Tsukuba, 305 JAPAN

(*1) For comprehensive reviews, the reader who is interested in the former two methods is referred to Bengtsson (1975) and who is interested in the NMI is to Daley (1981).

(1985a,b) and by Ballish and Sela (1985). Kudo (1984) proposed a new iteration method which was similar to the method of Rasch (1985b). It appears to be more robust than Rasch's method but, unfortunately, its characteristics have not been described in detail. Another initialization method called the bounded derivative method (Browning et al., 1980) also fails to converge in these cases (Ballish and Baer, 1985).

In addition, it is difficult in limited-area models to define normal modes which satisfy time-dependent boundary conditions. Progress in relieving this difficulty is being made (Bourke and McGregor, 1983; Juvanon du Vachat, 1986).

Recently, a method, simpler than NMI in concept, was proposed by Bratseth (1982) and was applied to a global forecast model successfully by Sugi (1986). All physical processes used in the model were taken into account through the initialization but no problem of convergence was found. The procedure of this method is summarized as follows: 1) integrate the model equations in a forward/backward cycle with a selective damping scheme such as the Euler-backward or Okamura's scheme (for these schemes, see Haltiner and Williams, 1982), 2) during the integration cycle, keep the nonlinear terms constant, and 3) after integration cycles, update the nonlinear terms and repeat the integration cycle and the nonlinear updating. This method is, therefore, a variation of dynamic initialization. Sugi (1986) also proved that this method is equivalent to NMI with a frequency dependent underrelaxation factor, and named it "dynamical normal mode initialization" (hereafter, we abbreviate it to DNI following Sugi). The old version of dynamic initialization was also capable of eliminating high-frequency gravity waves from the initial field of a hemispheric model (Temperton, 1973, 1976). It used, however, much more computational time than DNI because the nonlinear terms were updated at each forward/backward integration.

In this paper, DNI will be applied to a limited-area model. As Anthes (1983) pointed out, physical processes are important in a limited-area model. In some limited-area models, NMI is already used (as remarked early in this section) and has succeeded in eliminating gravity oscillations. Only few vertical modes, however, are initialized without irreversible processes because of the convergence problem. Highly diabatic phenomena such as heavy rainfall associated with a cold front may be suppressed by the adiabatic NMI as the Hadley circulation and tropical depressions were suppressed by it in global models (*e.g.* Kitade, 1983; Rasch, 1985b). Therefore, DNI, in which the problem of convergence was not found in the examination by Sugi (1986), is an attractive method. In addition, the normal modes are not calculated in DNI and, therefore, the boundary problems associated with this are absent.

The choice of time integration scheme governs the efficiency and the stability of DNI. From these view points, we shall discuss two schemes: Okamura's scheme and a backward implicit scheme. In the case of the backward implicit scheme, it will be shown that we have to evaluate implicitly even the nonlinear terms to perform the integration cycle stably. By estimating the nonlinear terms approximately, we will show some numerical results and compare with the results of NMI.

2. Time integration scheme for DNI

As mentioned in section 1, it is important for DNI to choose an efficient time integration scheme. In this section, we discuss the efficiency and the stability of two selective damping schemes: Okamura's scheme and a backward implicit scheme. First, their linear characteristics are examined and, next, the effects of nonlinear terms are evaluated.

2.1 Linear characteristics

(a) Okamura's scheme

This scheme proposed by Okamura (Haltiner and Williams, 1980), which was used to initialize the FSU global model by Sugi (1986), consists of a forward step, a backward step, and an extrapolation.

$$\begin{cases} u_*^{t+\Delta t}=u_n^t+\Delta t(\partial_t u_n)^t, \\ u_{**}^t=u_*^{t+\Delta t}-\Delta t(\partial_t u_*)^{t+\Delta t}, \\ u_{n+1}^t=3u_n^t-2u_{**}^t, \end{cases} \tag{2.1}$$

where Δt is the time step, ∂t is the time derivative, n is the number of the integration cycle. The linear response function of one cycle forward-backward integration is

$$R_L(\omega)=\frac{u_{n+1}^t}{u_n^t}=1-2(\omega\Delta t)^2, \tag{2.2}$$

where only the linear terms are considered and ω is the frequency of the normal mode.

A necessary condition to complete the integration cycle stably is given by

$$|R_L(\omega_{\max})|\leqq 1, \tag{2.3a}$$

where $\omega_{\max}$ is the maximum frequency of the model normal modes. The condition (2.3a) is rewritten as

$$0\leqq\omega_{\max}\Delta t\leqq 1. \tag{2.3b}$$

For the model used (for the brief description of the model, see the next section), $\omega_{\max}$ is estimated as

$$\omega_{\max}\approx\frac{2\sqrt{2}C_{p\max}}{\Delta x_{\min}}, \tag{2.4}$$

where $C_{p\max}$ is the maximum phase velocity of the model normal modes ($\sim$ 300m/sec), and $\Delta x_{\min}$ is the minimum grid size of the model ($\sim$ 30km). Thus (2.3) becomes

$$0\leqq\Delta t\leqq 35\,\text{sec}. \tag{2.5}$$

The damping factor after n integration cycles is given as

$$\mu(\omega)=|R_L(\omega)|^n=|1-2(\omega\Delta t)^2|^n. \tag{2.6}$$

Therefore, in order to reduce the amplitudes of fast oscillations whose periods are less than 2 hours, for example, to be less than one fourth of the initial value, we must complete at least 740 cycles. The damping factor $\mu(\omega)$ in this case is shown in Fig. 1 by the dashed line.

The fact that many integration cycles must be performed to reduce the fast oscillations indicates an inefficiency in Okamura's scheme for limited-area models, which was also mentioned in Sugi (1986). The inefficiency can be described another way as follows. Choosing $\Delta t=\omega_{\max}^{-1}$, the number of cycles needed is

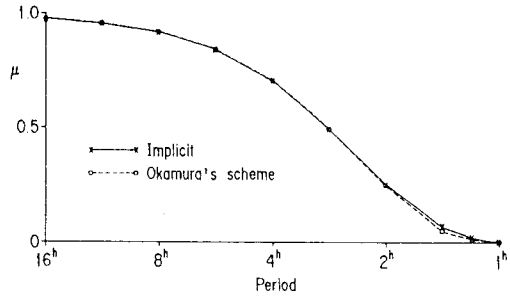

Fig. 1. Damping characteristics of Okamura's scheme with $n=740$ (dashed line) and of the implicit scheme with $n=32$ (solid line).

rewritten as

$$n=\frac{\log\mu(\omega_c)}{\log\{|1-2(\omega_c/\omega_{\max})^2|\}}, \tag{2.7}$$

where ω_C is the frequency to be reduced. The curve (2.7) is graphed in Fig. 2 and the number of cycles needed for the global model used by Sugi (1986) and for the limited-area model we use are indicated in the figure by FSUGCM and PERIDOT, respectively. Using (2.4), we can estimate the number approximately as

$$n\propto\frac{C_{p\max}\log\mu^{-1}}{(\Delta x_{\min})^2\omega_c^2}. \tag{2.8}$$

Thus, the number of integration cycles is very sensitive to the grid size. Usually, $\Delta x_{\min}$ in the limited area model is smaller than that in the global model and, therefore, the efficiency of Okamura's scheme is much reduced.

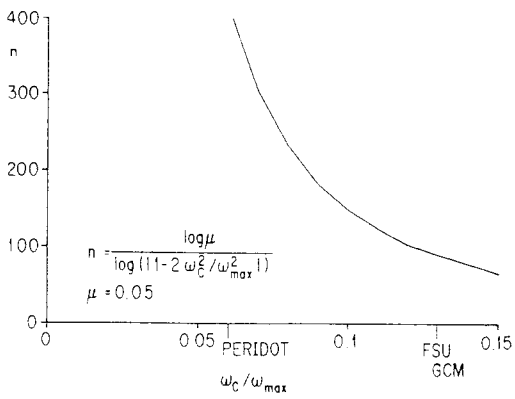

Fig. 2. Number of necessary integration cycles as a function of the ratio $\omega_C/\omega_{\max}$.

In the model we used, the computation time on a CRAY-1 is 0.6 sec for one cycle of Okamura's scheme; 440 sec to integrate 740 cycles. This is longer than the computational time for a 12 hour forecast by the model.

(b) Backward implicit scheme

To overcome the problem of Okamura's scheme described above, consider the backward implicit scheme:

$$\begin{cases} u_*^{t+\Delta t}=u_n^t+\Delta t(\partial_t u_*)^{t+\Delta t}, \\ u_{n+1}^t=u_*^{t+\Delta t}-\Delta t(\partial_t u_{n+1})^t. \end{cases} \tag{2.9}$$

The linear response function of one cycle of integration is

$$R_L(\omega)=\{1+(\omega\Delta t)^2\}^{-1}, \tag{2.10}$$

and the scheme (2.9) is unconditionally stable. As far as linear terms are considered, no condition for Δt is imposed, and it permits us to decrease the number of integration cycles n. In fact for $\Delta t=240$ sec, n is only 32 and almost the same damping characteristics as in the previous subsection are obtained. The damping factor for n=32 and $\Delta t=240$ sec is also shown in Fig. 1 by the solid line.

2.2 Effects of nonlinear terms

By considering the effects of nonlinear terms in a simple manner, we can derive more precise response functions and necessary conditions for the time step Δt. As a first step, we rewrite the governing equations of atmospheric motion as

$$\partial_t a_j=i\omega_j a_j+r_j(a_1, a_2, \cdots, a_n), \tag{2.11}$$

where a_j and ω_j are the amplitude and the frequency of the j th normal mode respectively, and r_j is the nonlinear term. Eqation (2.11) is derived by a proper linear transformation (*e.g.* Daley, 1981). If we presume that a_j is of the form

$$a_j=\chi_j\exp[(i\sigma_j-a_j)t], \tag{2.12}$$

where σ_j and α_j are the frequency and damping index when the nonlinearity is included, then (2.11) can be rewritten as

$$r=\{i(\sigma-\omega)-\alpha\}a, \tag{2.13}$$

where the subscript j is dropped.

We may now derive response functions and the conditions for Δt.

(a) Okamura's scheme

With (2.11)~(2.13), the integration cycle (2.1) is rewritten as

$$\begin{cases} \chi_*^{t+\Delta t}=\chi_n^t\{1+\Delta t(i\sigma-\alpha)\}, \\ \chi_{**}^t=\chi_*^{t+\Delta t}(1-i\omega\Delta t)-\Delta t\{i(\sigma-\omega)-\alpha\}\chi_n^t, \\ \chi_{n+1}^t=3\chi_n^t-2\chi_{**}^t, \end{cases} \tag{2.14}$$

where the nonlinear term is not changed in the cycle. The response function is

$$R_N(\omega)=1-2\omega(\sigma+i\alpha)\Delta t^2. \tag{2.15}$$

The stability condition $|R(\omega)|\leqq 1$ is written as

$$\Delta t^2\leqq\left\{\omega\sigma\left(1+\frac{\alpha^2}{\sigma^2}\right)\right\}^{-1}, \tag{2.16}$$

Further, we can rewrite (2.16) as

$$\omega\sigma\geqq 0, \tag{2.17a}$$

and

$$\bar{\omega}\Delta t\leqq 1, \tag{2.17b}$$

where

$$\bar{\omega}=\sqrt{\omega\sigma\left(1+\frac{\alpha^2}{\sigma^2}\right)},$$

is a frequency modified by the nonlinearity.

The condition (2.17a) indicates that the scheme will be unstable if the frequency σ has the opposite sign to the frequency of the corresponding normal mode ω. A breakdown of (2.17a) would occur if wind is strong and the Doppler-shifted frequency has the opposite sign. On the other hand, (2.17b) is the same form as (2.3b) except $\omega_{\max}$ is replaced by $\bar{\omega}$. Since $\bar{\omega}$ could be larger than $\omega_{\max}$ by, for example, the Doppler shift, (2.17b) restricts the time step to shorter than (2.3b).

(b) Backward implicit scheme

Explicit evaluation of the nonlinear term.

Using (2.11) and (2.12), the integration cycle (2.9) is rewritten as

$$\begin{cases}\chi_*^{t+\Delta t}=\chi_n^t+i\omega\Delta t\chi_*^{t+\Delta t}+\Delta t\{i(\sigma-\omega)-\alpha\}\chi_n^t, \\ \chi_{n+1}^t=\chi_*^{t+\Delta t}-i\omega\Delta t\chi_{n+1}^{t+\Delta t}-\Delta t\{i(\sigma-\omega)-\alpha\}\chi_n^t, \end{cases} \tag{2.18}$$

where the nonlinear term is evaluated in an explicit manner.

The response function is

$$R_N(\omega)=\frac{1-\omega\{\sigma-\omega+i\alpha\}\Delta t^2}{1+\omega^2\Delta t^2}, \tag{2.19}$$

and the necessary condition for the stability is

$$|R_N|^2=\frac{\{1-\omega(\sigma-\omega)\Delta t^2\}^2+\alpha^2\omega^2\Delta t^4}{(1+\omega^2\Delta t^2)^2}\leqq 1. \tag{2.20}$$

To know the characteristics of the scheme (2.18), examine two extreme cases: zero nonlinear damping ($\alpha=0$) and zero modulation to the frequency ($\sigma=\omega$).

In the case of the zero damping, (2.20) becomes

$$\sigma(\sigma-2\omega)\Delta t^2\leqq\frac{2\sigma}{\omega}. \tag{2.21}$$

and, in the case of the zero modulation,

$$(\alpha^2-\omega^2)\Delta t\leqq 2. \tag{2.22}$$

The condition (2.21) is rather complicated and examination of it in detail would not be useful. The condition (2.22)is,on the other hand, simple and can be interpreted clearly: if the damping (or the amplifying) effect of the nonlinearity is strong enough (*i.e.* $\alpha^2>\omega^2$), a condition on Δt is imposed. In fact, it occurs in two cases, 0000UTC and 0600UTC 4 June 1986. In these cases, the term which parameterizes the turbulent vertical flux is large and a time step much smaller than 240 sec must be taken. It reduces the efficiency of the scheme.

Implicit evaluation of nonlinear term.

The integration cycle (2.9) is rewritten in this case as

$$\begin{cases}\chi_*^{t+\Delta t}=\chi_n^t+\Delta t(i\sigma-\alpha)\chi_*^{t+\Delta t}, \\ \chi_{n+1}^t=\chi_*^{t+\Delta t}-i\omega\Delta t\chi_{n+1}^t-\Delta t\{i(\sigma-\omega)-\alpha\}\chi_*^{t+\Delta t}. \end{cases} \tag{2.23}$$

The response function is

$$R_N(\omega)=\frac{1+\alpha\Delta t-i(\sigma-\omega)\Delta t}{(1+\alpha\Delta t-i\sigma\Delta t)(1+i\omega\Delta t)}. \tag{2.24}$$

We again examine the two extremes $\alpha=0$ and $\sigma=\omega$. In the case of zero damping $\alpha=0$, the necessary condition for the stability, $|R(\omega)|\leqq 1$, becomes

$$\sigma\omega\geqq 0. \tag{2.25}$$

This condition is the same as (2.17a)and it also means that the scheme will be unstable if, for example, wind is strong enough to reverse the sign of the frequency due to Doppler shift.

In the case of zero modulation, $\sigma=\omega$, the stability condition becomes

$$\left(\Delta t+\frac{\alpha}{\omega^2+\alpha^2}\right)^2+\frac{2\omega^2+\alpha^2}{(\omega^2+\alpha^2)^2}\geqq 0, \tag{2.26}$$

which is always satisfied insofar as all variables Δt, α, and ω are real.

In the following sections, we shall use the backward implicit scheme (2.9). The implicit evaluation of the nonlinear terms is best since no condition for the time step was found in the above analysis; it is difficult in practice, however. An approximate scheme to estimate the terms will be used, and the details of this scheme will be presented in Appendix A. We shall use the values $n=32$ and $\Delta t=240$ sec with nonlinear terms updating once every 8 integration cycles. The reason why these values are chosen will be explained later.

3. The meso-scale model

The three-dimensional forecast model used is a 15 σ-level, hydrostatic, limited-area model developed by the French Weather Service (see Imbard *et al.*, 1986, 1987; Bougeault, 1987; for the detailed description of the model). The forecast variables are surface pressure, horizontal wind, temperature, and specific humidity. The model includes the following physical processes: surface flux, vertical turbulent flux, radiation, clouds, and precipitation by deep cumulus convection and by large-scale condensation. In addition, land-surface processes are described by soil temperature and moisture using two levels.

Time integration uses a semi-implicit method with a leap-frog scheme and a low-pass filter (Asselin, 1972). The lateral boundary condition is the Davies (1976) relaxation method.

A 51 × 51 horizontal grid matrix, centered at 46°N 3°E, is used with a time step of 240 sec and a grid increment of 35km at the center.

4. Numerical experiment starting with real data.

In this section we will describe the characteristics of DNI with the backward implicit scheme and compare them with those of NMI. The initial data are the fine-mesh analysis of 0000UTC 4 June 1986. The preparation of the input data for the fine-mesh analysis and the details of the method of the analysis is described in Durand (1985), Imbard *et al.* (1986, 1987) and Durand and Bougeault (1987). The analyzed data have been prepared in the frame of the Hapex-Mobilhy project (André *et al.*, 1986) and are described by Mercusot *et al.* (1986). NMI of the model includes only adiabatic terms and uses Machenhauer's iteration scheme. It initializes the largest two vertical modes.(*2) The surface pressure and the temperature at the lowest layer of the model are not altered during initialization (see Brière, 1982; Craplet, 1985; for the detailed description of NMI of the model).

On the 4 June 1986, a cold front with accompanying precipitation was passing across central France as shown in Fig. 3a and strong wind was revealed, as shown in Fig. 3b. This situation would be severe on both NMI and DNI, because NMI in the model does not include diabatic processes at all and because DNI may be unstable in this strong wind condition.

4.1 Convergence of integration cycle

Figure 4 shows the mean square rate of surface pressure change

$$B(p_s)=\overline{(\partial_t \ln p_s)^2}, \qquad (4.1)$$

where p_s is surface pressure, versus the number of integration cycles. Although we use an approximation to the exact implicit evaluation of the nonlinear terms as described in the Appendix A, the shocks by the nonlinear-term updating are small and $B(p_s)$ decreases rather smoothly by two orders.

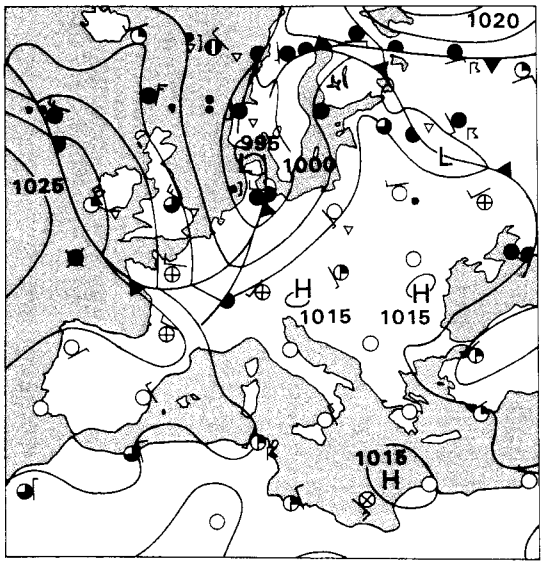

(a)

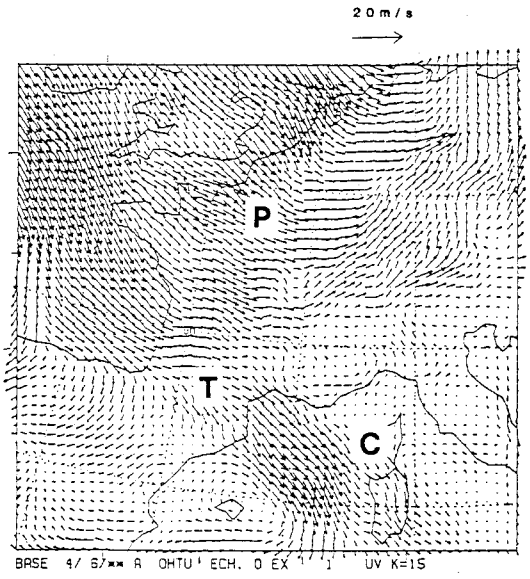

(b)

Fig. 3. The initial atmospheric state at 0000UTC 4 June 1986. (a) Synoptic chart, (b) horizontal wind at the lowest layer of the model produced by the fine-mesh analysis.

(*2) The reason why NMI in the model initializes only two vertical modes is to avoid large modification of observed surface data. If it is needed, the number of the vertical modes can be increased to four, at least (Juvanon du Vachat, personal communication).

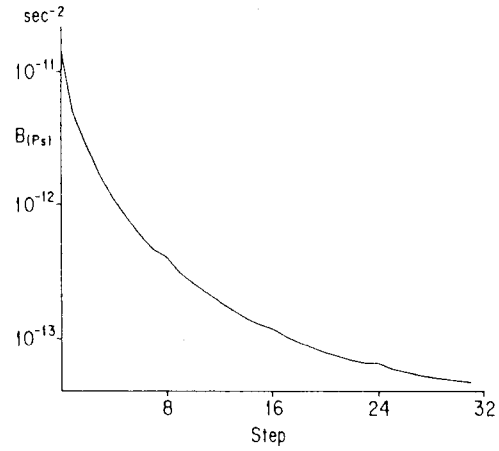

Fig. 4. Measure of balance $B(p_s)$ as a function of the number of integration cycles.

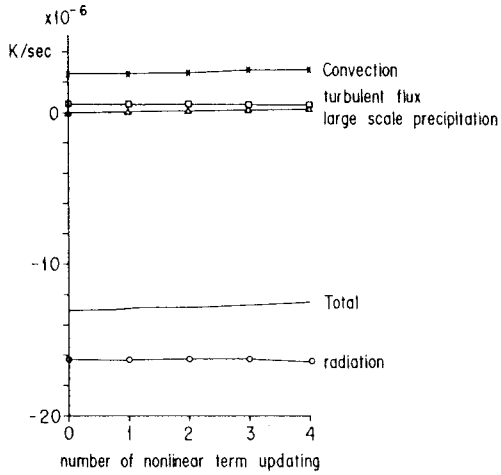

Fig. 5. Diabatic heating rate as a function of the number of nonlinear term updatings.

Figure 5 shows volume-averaged diabatic heating rate for each nonlinear term updating. It is nearly constant in this case and indicates that updating 4 times is sufficient for obtaining the converged state.

The degree of balance is represented by an index BAL:

$$BAL=\sum_j |\partial_t Z_j|^2, \tag{4.2}$$

where Z_j is the amplitude for a gravity mode and the summation is taken over all gravity modes. Figure 6 shows BAL after NMI with four iterations and BAL after DNI. While NMI shows

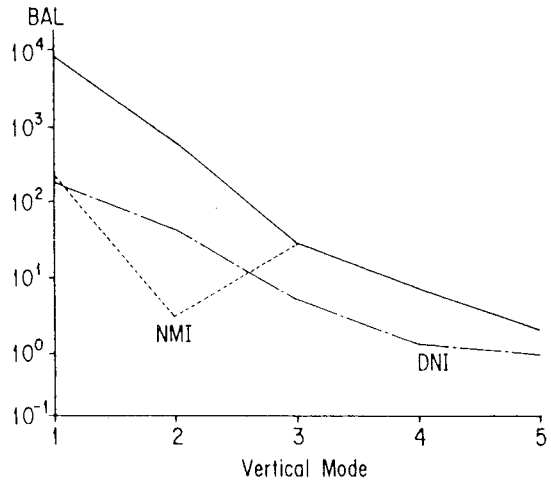

Fig. 6. Measure of balance BAL as a function of vertical mode. The value before the initialization is indicated by the solid line.

a good balance at the second vertical mode, DNI and NMI have almost the same BAL at the first mode. At the higher modes, DNI shows good balance because it initializes all vertical modes, in contrast to NMI which initializes only the first two modes.

4.2 Surface pressure

Figure 7 shows the time variation of surface pressure at three points: Paris, Toulouse, and the coast of the Corsica Island, which are marked in Fig. 3b by P, T, and C, respectively. The fast oscillations which have amplitudes 4~5 hPa and periods 0.7~2 hours are eliminated by both DNI and NMI. The initial surface pressure is modified by 1~2 hPa by DNI, since DNI does not fix surface pressure nor the lowest-layer air temperature. These quantities are, however, not altered during NMI of the model.

After 6 forecast hours, the fast oscillations are damped also by the model itself even if we do not initialize the data, and the surface pressure is almost the same as that of DNI and NMI.

5. Data-simulation experiment.

In the previous section, it was shown that DNI eliminated high-frequency gravity waves. It was not shown, however, that the physical quantities after DNI were the desired ones, that is,

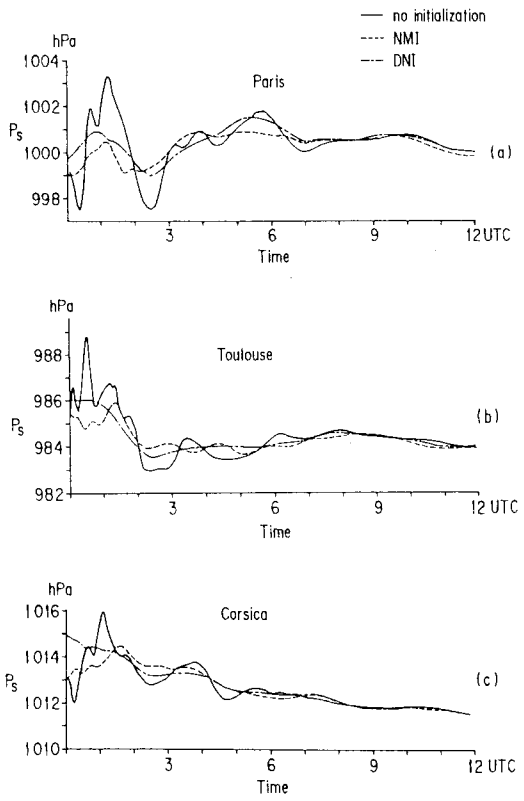

Fig. 7. Time variation of surface pressure (a) at Paris, (b) at Toulouse, and (c) at the coast of the Corsica Island, starting with real data.

comparable to real atmosphere values. Unless we observe the atmosphere perfectly, it is not possible to show it strictly. A method of avoiding the problem of the lack of observed data is so-called "identical-twin" method or "data-simulation" experiment. This method uses the control data simulated by the model instead of the observed data. We shall compare the data after DNI and NMI with the control atmosphere given by the simulation in the following sub-sections. An advantage of the method is that all data are given at the same time-space position, and, therefore, there is no problem in comparing them. But the results will be sensitive to the forecasting model itself, as well as to the initialization process.

A prerequisite to a meaningful experiment is that the control data are not affected by the initial conditions but are determined by the forecast model itself. As discussed in the previous section, differences due to the initialization schemes nearly disappeared after 6 forecast hours. The prerequisite, therefore, appears to be satisfied and one may perform the experiment as follows: as a control experiment, use the 6 to 12 forecast hours based on the initial data from 0000UTC 4 June 1986 with NMI. Also, regard the forecast for 0600UTC as the "perfect" initial data and the forecast by the control experiment then represents the "perfect" forecast.

To provide a smoothing effect by an objective analysis and to imitate imbalances among physical variables, we take 9 x 9 points average for horizontal wind for the perfect initial data, and, then, we initialize the averaged data by DNI or NMI. Finally, we compare the 6-hours forecast (*i.e.* from 0600 to 1200UTC), starting from the averaged-initialized data, with the control forecast. By this averaging, the wind data lose structures smaller than 300km; this is greater than the resolution of the fine-mesh analysis of the model (~100km). Therefore, for initialization schemes, this experiment may be a more severe test than in real situation.

5.1 Surface pressure

Figure 8 shows time variation of surface pressure at three points. Both initialization methods eliminate fast oscillations, as in the previous section. Although the initial surface pressure given by the DNI differs 0.2~0.5hPa from that by the control and the NMI, the forecast of the surface pressure with DNI is not worse than NMI.

5.2 Horizontal wind

Figure 9 shows the initial horizontal wind in the lowest layer, where the effects of mountains are most significant. Using the 9 x 9 points average, small structures represented in the perfect data (Fig. 9a) have disappeared as shown in Fig. 9b; this is most evident near the mountains in the Alps and the Pyrenees. We find that the lowest-layer wind is improved little by NMI (Fig. 9c) because NMI initializes only the first two vertical modes. By DNI, on the other hand, the deformation of the wind due to the mountains is reconstructed to a certain extent

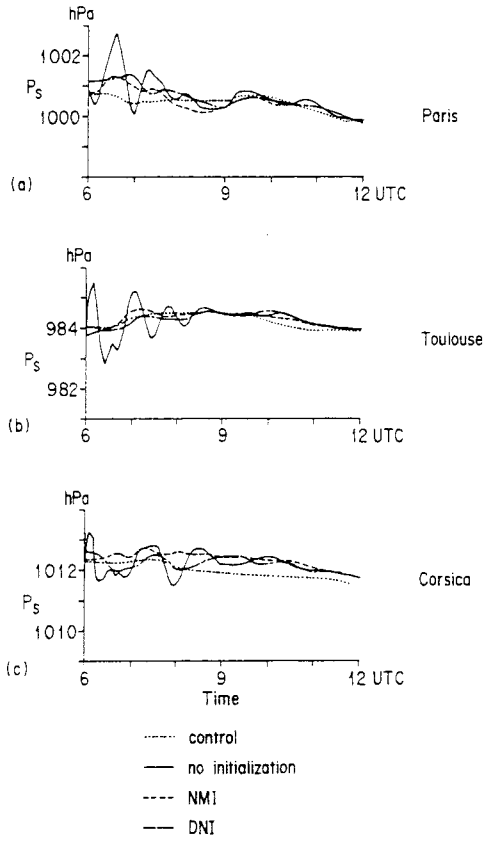

Fig. 8. As in Fig. 7, except for the simulation-data experiment.

(Fig. 9d). The improvement is still inadequate, but complete reconstruction is not possible unless the wind field is forced to adjust the pressure field, for example. The result, however, indicates that, in order to reconstruct the wind over mountains, higher vertical modes should be included in the initialization. In the problem of the inclusion of the surface friction, the necessity of higher vertical modes is also reported by Ballish and Baer (1985).

At higher levels, the difference between DNI and NMI is much smaller, and the rms error ER from the perfect data for the whole domain is nearly the same:

$$ER_u = 1.131 \text{ m/sec}, \quad ER_v = 1.117 \text{ m/sec},$$

for DNI, and

$$ER_u = 1.185 \text{ m/sec}, \quad ER_v = 1.174 \text{ m/sec},$$

for NMI.

5.3 Precipitation

Time variation of the area-averaged precipitation rate is shown in Fig. 10a. The averaged precipitation rate in the first hour after DNI is intermediate between the perfect forecast and the adiabatic NMI. Subsequently, the mean precipitation rate recovers quickly in both experiments. The underestimation of precipitation by DNI is mainly due to the averaging process used, because it almost disappears in the case where the perfect data is initialized by DNI (closed circle in Fig. 10a). The result that the forecast with NMI, which includes only adiabatic terms, for the perfect data underestimaes the precipitation (closed square in Fig. 10a) indicates the importance of the inclusion of physical processes in initialization process.

Figure 10b shows the rms error from the control experiment for the precipitation. The forecast of the first three hours after DNI is better than that after NMI, while the difference disappears after the 4 hours forecast.

Figures 11b and 11c show differences of the precipitation in the first one hour after DNI and after NMI, respectively, from the control experiment (Fig. 11a). Both forecasts with DNI and NMI underestimate the maximum precipitation, but the difference from the control experiment is smaller in the forecast with DNI than that with NMI.

5.4 Computation time and stability of DNI.

The computation time (CPU time) of the implicit DNI for the operational model of the French Weather Service is around 30 sec on the CRAY-2 for the case of nonlinear updating 4 times in 32 integration cycles. It is about 3 times larger than that of the adiabatic NMI with 4 iterations of 2 vertical modes ($\sim$10 sec). While the difference on CPU time is large, this is not a grave defect of DNI if we weigh the difference of the two methods: NMI includes only adiabatic processes while DNI includes all processes in the model.

A defect rather more serious than the CPU time consumption is the instability suggested by (3.25). Figure 12 shows the difference in

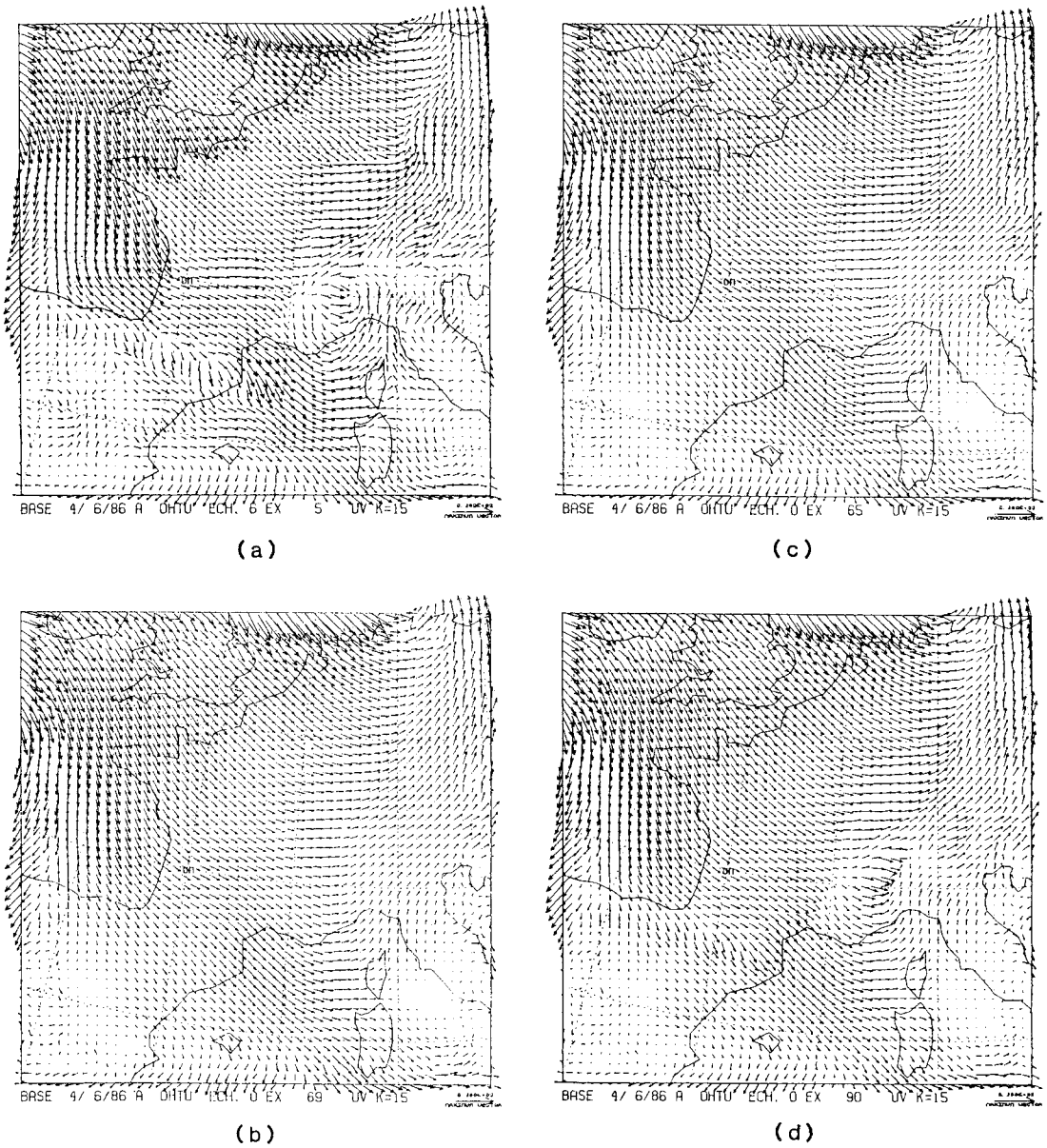

Fig. 9. Horizontal wind in the lowest layer of the model at the initial time (0600UTC). (a) The "perfect" initial data, (b) after 9×9 points averaging, (c) after averaging and NMI, and (d) after averaging and DNI.

lowest-layer air temperature ΔT_{15} between the "perfect" initial data and the data after DNI following the average of the horizontal wind:

$$\Delta T_{15}=T_{15,\,\mathrm{perfect}}-T_{15,\,DNI}\,.$$

We observe signs of the instability characterized by a pattern like a checkerboard over the Mediterranean Sea. Although the amplitude of the instability is largest for T_{15}, it is only about 0.25~0.5℃. It contaminates the initialized field only a little, as shown in Fig. 13.

If we increase the time step Δt of the integration cycles, we can decrease the number of the cycles and the CPU time. The amplitude

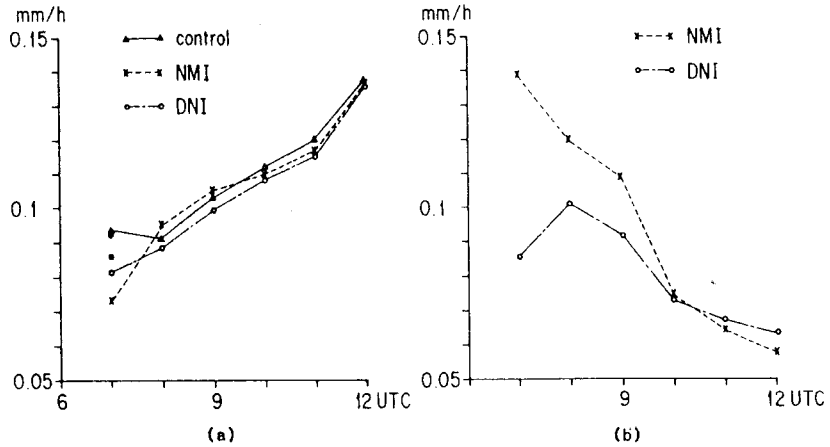

Fig. 10. (a) Time variation of the area-averaged precipitation. Closed circle and square indicate the area-averaged precipitation for the first on hour after DNI and NMI with the perfect data, respectively.
(b) Time variation of the rms error of precipitation from the control experiment.

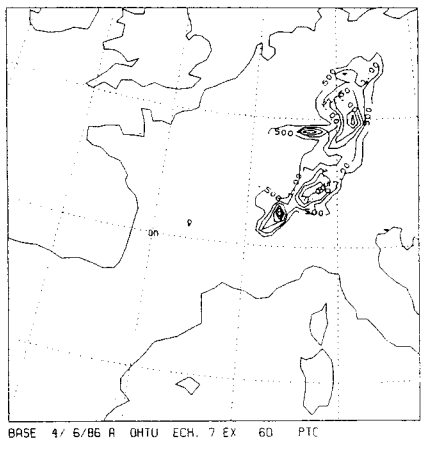

(a)

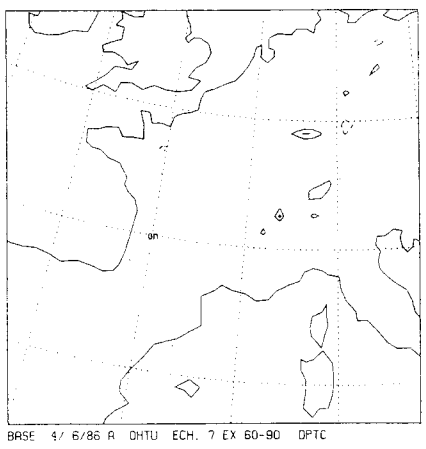

(b)

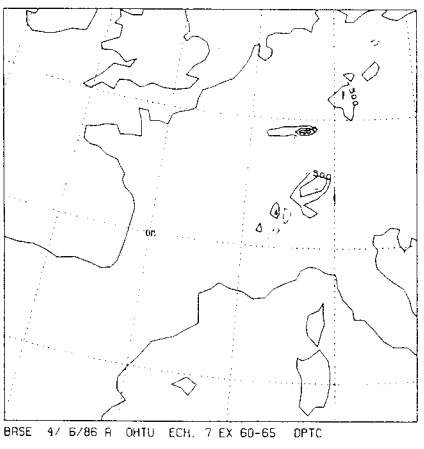

(c)

Fig. 11. (a) Precipitation for the first one hour by the control experiment; (b) difference of the precipitation of the first one hour between the control experiment and the experiment with DNI; (c) with NMI. The contour interval is 0.5mm and the dashed lines indicate negative values.

of the checkerboard pattern, however, increases (the dependence of the response function on Δt is evaluated in Appendix B). The region contaminated by the instability also extends. Therefore, we choose the values Δt=240 sec, n=32 at the sacrifice of the CPU time.

6. Summary and discussion

We have applied the dynamic normal mode

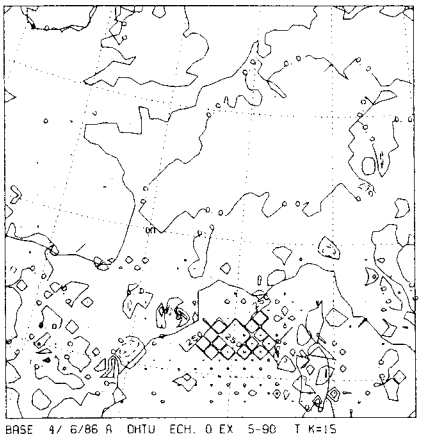

Fig. 12. Difference of the initial air temperature at the lowest layer between the "perfect" initial data and the data after DNI following the averaging. The contour interval is 0.25℃ and the dashed lines indicate negative values.

initialization to the French limited-area model. Because of the inefficiency of Okamura's scheme, we used the backward implicit scheme for the time integration cycle. After 32 cycles of integration with the nonlinear terms, updating 4 times, fast oscillations were successfully damped.

The computation time of DNI (~30 sec) was almost 3 times larger than NMI. This might not be a grave disadvantage because only 2 vertical modes are initialized by adiabatic NMI. If more vertical modes, for example 5 or 6 modes, are initialized by NMI(*3), the CPU time would be nearly the same.

By the "identical twin" method, the horizontal wind and the precipitation rate were compared among the control experiment, the experiment starting with NMI, and the experiment with DNI. The deformation of the lowest-layer wind due to the mountains was reconstructed through DNI better than NMI,but the improvement was not sufficient. It was also shown that the rms error of the precipitation from the control experiment was smaller in the experiment with DNI than that with NMI for the first 3 hours. The area-averaged precipitation was

(*3) In order to resolve an Ekman type circulation through NMI, all vertical modes must be initialized (Ballish and Baer, 1985). It is 15 for the French limited-area model.

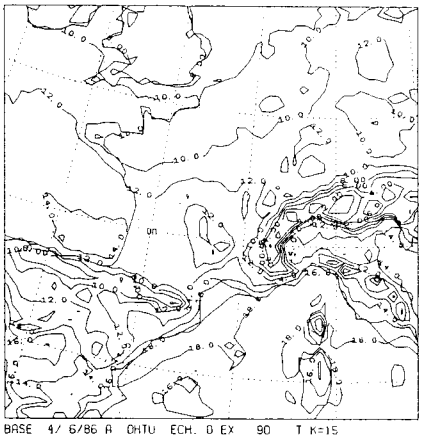

Fig. 13. (a) The air temperature at the lowest layer in the "perfect" data, and (b) after DNI.

also improved by DNI.

In spite of the above improvement using DNI, there is a discrepancy between the perfect forecast and the forecast after DNI. Two possible reasons for the difference between the perfect forecast and the experiment with DNI are: 1) due to the averaging process used, the structure which accounts for a certain amount of precipitation was lost, and the initialization process could not reconstruct it; 2) since the time integration scheme in DNI (implicit scheme) is different from that of the forecast model (semi-implicit leap-frog scheme), the balanced state after DNI would be different from that of the forecast model. The former problem is less

severe in a real situation because the fine mesh analysis for this model has better resolution than the averaged data. The latter is, however, inevitable for DNI because DNI has to use the selective damping scheme whose cut-off frequency is low enough for the time integration schemes of the forecast model to permit the wave propagating neutrally. NMI or VMI (Bourke and McGregor, 1983) with physical processes would be better if the iteration converges, because they can use the same time difference scheme as the forecast model. The balance condition of the iteration in NMI, however, has been suggested as being different from the model balance condition (Rasch, 1985b), especially for low frequency modes (Errico, 1984). Therefore, as long as a good iteration method for VMI or NMI is not found, DNI has the advantage that we can include any physical process with small risk of divergence.

We have compared DNI and NMI only in rainy weather. Certainly, it is not sufficient to conclude which method is practically best for the initialization of short-range (from a few hours to one day) forecasts by meso-scale numerical models. We also have to examine other synoptic conditions of fair weather. In addition, we have to compare the numerical results not only with the data by the identical twin method but also with the fine-mesh analysis of observed data. In the case of rainy weather, the precipitation or other variables related to latent heat release will be good indices to examine the performance of the initialization method, since then the differences among initialization method will be most significant, as reported in Salmon and Warner (1986) and in Zhang and Fritsch (1986). In the case of fair weather, other variables such as the surface heat flux or the shear vector in the mixing layer are possibly good indices. Those are left to further study.

Another candidate for which DNI is suitable would be models for small-scale phenomena. For such phenomena, the diabatic processes (condensation, surface flux, etc.) would be most important, and all vertical modes should be initialized with diabatic processes. The current iteration method in NMI might not converge under such condition. The integration cycle in DNI, however, could be performed stably. The application of DNI to a model with Δx=10km is now being tested.

Acknowledgments

The author would like to thank P. Bougeault for the encouragement through this work as well as for many valuable comments and discussions. C. Mercusot provided the fine-mesh analysis data and supported the programming. P. Lacarrere prepared graphic programs. The author is indebted to R. Juvanon du Vachat, R. Daley, J. Noonan, and the anonymous reviewers for their constructive criticisms and suggestions.

The computations were carried out at Direction de la Météorologie Nationale, Paris, and at Centre de Calcul Vectoriel pour la Recherche, Palaiseau, France.

This research was conducted during the author's visit to Centre National de Recherches Météorologiques under the auspices of Science and Technology Agency, Tokyo, Japan.

Appendix A

Detail of the implicit integration cycle

To obtain the desired characteristics shown in section 2.2, we have to calculate the nonlinear terms by the implicit method. It is difficult, however, to calculate them strictly. Therefore, we estimate the terms roughly as described below.

The governing equations are rewritten as

$$\begin{cases} \partial_t u+\partial_x P=N_u, \\ \partial_t v+\partial_x P=N_v, \\ \partial_t T+\dfrac{R_a\overline{T}}{c_{pa}}\dfrac{1}{\sigma}\displaystyle\int_0^{\sigma}(\partial_x u+\partial_y v)d\sigma=N_T, \\ \partial_t Z+\displaystyle\int_0^{1}(\partial_x u+\partial_y v)d\sigma=N_z, \end{cases} \quad \text{(A.1)}$$

where u and v are horizontal wind, $P=\hat{\phi}+R_a\overline{T}Z$, $\hat{\phi}$ the geopotential of dry air, R_a and c_{pa} are the gas constant and the specific heat respectively, $\overline{T}$ the horizontally averaged temperature, $Z=\ln(p_s)$, p_s the surface pressure, T the temperature, $\sigma=p/p_s$, and the subscribed quantities N denote nonlinear terms and other residual terms not included in the left-hand-sides. The separation of

the linear and the nonlinear (and the residual) terms is exactly the same as that of the semi-implicit scheme of the model. It should be noted that the Coriolis terms are taken onto the right-hand sides. As far as this separation is used in the time integration of the forecast model, no problem has been experienced. We do not prove analytically that it works well in the forward/backward cycle, but, in the case examined, we again experienced no problem.

For simplicity, we rewrite (A.1) as

$$\partial_t \boldsymbol{X} + \boldsymbol{L}(\boldsymbol{X}) = \boldsymbol{N}(\boldsymbol{X}) , \tag{A.2}$$

where $\boldsymbol{X}$ is the physical quantity, $\boldsymbol{L}$ and $\boldsymbol{N}$ represent the linear and the nonlinear terms respectively. Then, the implicit method in (2.23) is written as

$$\boldsymbol{X}_*^{t+\Delta t} = \boldsymbol{X}_n^t - \Delta t \boldsymbol{L}(\boldsymbol{X}_*^{t+\Delta t}) + \Delta t \boldsymbol{N}(\boldsymbol{X}_*^{t+\Delta t}) , \tag{A.3a}$$

$$\boldsymbol{X}_{n+1}^t = \boldsymbol{X}_*^{t+\Delta t} + \Delta t \boldsymbol{L}(\boldsymbol{X}_{n+1}^t) - \Delta t \boldsymbol{N}(\boldsymbol{X}_*^{t+\Delta t}) . \tag{A.3b}$$

As mentioned at the beginning of this appendix, it is difficult to perform the integration (A.3a) owing to the implicit nonlinear term. We avoid this difficulty by estimating the value using an approximate value of $\boldsymbol{X}_*^{t+\Delta t}$ as follows:

(i) Integrate the linear term implicitly and the nonlinear term explicitly for one step as

$$\hat{\boldsymbol{X}}^{t+\Delta t} = \boldsymbol{X}_n^t - \Delta t \boldsymbol{L}(\hat{\boldsymbol{X}}^{t+\Delta t}) + \Delta t \boldsymbol{N}(\boldsymbol{X}_n^t) , \tag{A.4}$$

where the implicit calculation for the linear term is easily performed by modifying the semi-implicit scheme of the model.

(ii) Regarding $\hat{\boldsymbol{X}}^{t+\Delta t}$ as an approximate value of $\boldsymbol{X}_*^{t+\Delta t}$, we complete the integration cycle as

$$\boldsymbol{X}_*^{t+\Delta t} = \boldsymbol{X}_n^t - \Delta t \boldsymbol{L}(\boldsymbol{X}_*^{t+\Delta t}) + \Delta t \boldsymbol{N}(\hat{\boldsymbol{X}}^{t+\Delta t}) ,$$

$$\boldsymbol{X}_{n+1}^t = \boldsymbol{X}_*^{t-\Delta t} + \Delta t \boldsymbol{L}(\boldsymbol{X}_{n+1}^t) - \Delta t \boldsymbol{N}(\hat{\boldsymbol{X}}^{t+\Delta t}) . \tag{A.5}$$

Since we perform the step (i) only when the nonlinear term is updated, the additional computational time is not large.

The response function of this estimation scheme can be derived straightforwardly by the same method as that in the section 2.2. The result is not shown because of its complexity.

Appendix B

Dependence of the response function on Δt

By including the effect of the finite time step Δt in the estimation of the nonlinear term (2.13), we can estimate the dependence of the nonlinear response function on Δt in the case $|\omega \Delta t| \ll 1$ and $|\sigma \Delta t| \ll 1$.

Equation (2.11) is rewritten as

$$\frac{a^{t+\Delta t} - a^t}{\Delta t} = i\omega a^{t+\Delta t} + r , \tag{B.1}$$

where the subscript j is dropped and the backward implicit scheme is used. By assuming (2.12) and $\alpha_j = 0$, (B.1) is rewritten as

$$r = i\left\{\frac{\sin(\sigma \Delta t/2)}{\Delta t/2} e^{i\sigma \Delta t/2} - \omega\right\} a^{t+\Delta t} , \tag{B.2}$$

which corresponds to the finite difference form of (2.13). Assuming $|\sigma \Delta t| \ll 1$, the right-hand-side of (B.2) is approximated as

$$r = i\left\{\sigma\left(1 - \frac{i\sigma \Delta t}{2}\right) - \omega\right\} a^{t+\Delta t} . \tag{B.3}$$

Using (B.3), the response function (2.24) becomes

$$R = \frac{1 - (\sigma^2 \Delta t^2/2) - i(\sigma - \omega)\Delta t}{(1 - (\sigma^2 \Delta t^2/2) - i\sigma \Delta t)(1 + i\omega \Delta t)} \tag{B.4}$$

and it is approximated as

$$R = 1 - \Delta t^2 \sigma(\sigma + \omega) , \tag{B.5}$$

where $|\omega \Delta t| \ll 1$ and $|\sigma \Delta t| \ll 1$ are assumed. This equation indicates that the scheme (2.23) is unstable if $\sigma\omega < 0$ and $|\sigma| < |\omega|$. It also indicates that the amplification factor defined by $|R-1|$ is proportional to Δt^2.

References

André, J. C., J. P. Goutorbe and A. Perrier, 1986: Hapex-Mobilhy: A hydrologic atmospheric pilot experiment for the study of water budget and evaporation flux at the climate scale. *Bull. Amer.*

Meteor. Soc., **67**, 138-144.

Anthes, R.A., 1983: Regional models of the atmosphere in middle latitudes. *Mon. Wea. Rev.*, **111**, 1306-1335.

Asselin, R., 1972: Frequency filter for time integrations. *Mon. Wea. Rev.*, **100**, 487-490.

Ballish, B.A. and F. Baer, 1985: Normal mode initialization with elementary surface friction. *Mon. Wea. Rev.*, **113**, 241-247.

————, and J.G. Sela, 1985: Including physics in the normal mode initialization of the NMC spectral model. *Proceeding of 7th Conf. Numerical Weather Prediction, Amer. Meteor. Soc.*, 121-124.

Bengtsson, L., 1975: 4-dimensional assimilation of meteorological observations. *GARP Pub. Ser.* No. 15, WMO/ICSU Joint Organizing Committee, 76pp.

Bijlsma, S.J., and L.M. Hafkenscheid, 1986: Initialization of a limited area model: A comparison between the nonlinear normal mode and bounded derivative methods. *Mon. Wea. Rev.*, **114**, 1445-1455.

Bougeault, P., 1986: Le modèle PERIDOT: Une étude de qualification à méso-échelle. *Note de travail de l'EERM.* No. 168(#1).

Bourke, W., and J.L. McGregor, 1983: A nonlinear vertical mode initialization scheme for a limited area model. *Mon. Wea. Rev.*, **111**, 2285-2297.

Bratseth, A.M., 1982: A simple and efficient approach to the weather prediction models. *Tellus*, **34**, 352-357.

Brière, S., 1982: Nonlinear normal mode initialization of a limited area model. *Mon. Wea. Rev.*, **110**, 1166-1186.

Browning, G., A. Kasahara, and H.O. Kreiss, 1980: Initialization of the primitive equations by the bounded derivative method. *J. Atmos. Sci.*, **37**, 1424-1436.

Craplet, A., 1985: Initialisation par modes normaux du modèle PERIDOT. *Note de travail de l'EERM.* No. 139(#1).

Daley, R., 1981: Normal mode initialization. *Rev. Geophys. Space Phys.*, **19**, 450-468.

Davies, H.C., 1976: A lateral boundary formulation for multi-level prediction models. *Quart. J. R. Meteor. Soc.*, **102**, 405-418.

Durand, Y., 1985: The use of satellite data in French high resolution analysis. *ECMWF workshop on high resolution objective analysis.* 24-26 June 1985.

————, and P. Bougeault, 1987: L'analyse objective PERIDOT: *Note de travail de l'EERM.* No. 193(#1).

Errico, R.M., 1984: The dynamical balance of a general circulation model. *Mon. Wea. Rev.*, **112**, 2439-2454.

Haltiner, G.J., and R.T. Williams, 1980: *Numerical prediction and dynamic meteorology*, John Wily & Sons, New York, 447pp.

Imbard, M., A. Joly, and R. Juvanon du Vachat, 1986: Le modèle de prévision numérique PERIDOT. Formulation dynamique et mode de fonctionnement. *Note de travail de l'EERM.* No. 161(#1).

————, R. Juvanon du Vachat, A. Joly, Y. Durand, A. Craplet, J.F. Geleyn, J.M. Audoin, N. Marie, and J. M. Pairin, 1987: The PERIDOT fine-mesh numerical weather prediction system: Description, evaluation and experiments. *Short- and medium-range numerical weather prediction.* Special volume of the *J. Meteor. Soc. Japan.*

Juvanon du Vachat, R., 1986: A general formulation of normal modes for limited-area models: Application to initialization. *Mon. Wea. Rev.*, **114**, 2478-2487.

Kitade, T., 1983: Nonlinear normal mode initialization with physics. *Mon. Wea. Rev.*, **111**, 2194-2213.

Kudo, T., 1984: Normal mode initialization for global models (in Japanese). *Normal mode initialization.* Report of the Electronic Computation Center, No. 30, Japan Meteorological Agency, Tokyo, Japan, 20-35.

Mercusot, C., P. Bougeault, and Y. Durand, 1986: Programme Hapex-Mobilhy. Atlas des analyse PERIDOT(#2).

Rasch, P.J., 1985a: Developments in normal mode initialization. Part I: A simple interpretation for normal mode initialization. *Mon. Wea. Rev.*, **113**, 1746-1752.

————, 1985b: Developments in normal mode initialization. Part II: A new method and its comparison with currently used schemes. *Mon. Wea. Rev.*, **113**, 1753-1770.

Salmon, E.M., and T. Warner, 1986: Short-term numerical prediction forecasts initialized using a diagnosed divergent-wind component. *Mon. Wea. Rev.*, **114**, 2122-2132.

Sugi, M., 1986: Dynamic normal mode initialization. *J. Meteor. Soc. Japan*, **64**, 623-636.

Temperton, C., 1973: Some experiments in dynamic initialization for a simple primitive equation model. *Quart. J. R. Meteor. Soc.*, 99, 303-319.

————, 1976: Dynamic initialization for a barotropic and multilevel models. *Quart. J. R. Meteor. Soc.*, **102**, 297-311.

Williamson, D.L., and C. Temperton, 1981: Normal mode initialization for a multilevel grid-point model. Part II: Nonlinear aspects. *Mon. Wea. Rev.*, **109**, 744-757.

Zhang, D.L., and J.M. Fritsch, 1986: A case study of the sensitivity of numerical simulation of mesoscale convective system to varying initial conditions. *Mon. Wea. Rev.*, **114**, 2418-2431.

(#1) Available from Direction de la Météorologie Nationale, 77 rue de Sevres, 92106, Boulogne, France.

(#2) Available from CNRM, 42 avenue G. Coriolis, 31057, Toulouse CEDEX, France.

局地モデルにおける力学的規準モード初期化法

里 村 雄 彦(*)
フランス国立気象研究センター

Sugiの提案した力学的規準モード初期化法（DNI）を局地モデルに適用し，その有効性を調べた。DNIを局地モデルに適用する場合，積分サイクルに用いるスキームとしてOkamuraのスキームは効率が悪く，インプリシット・スキームが良いことが示される。非線型項もインプリッシットにしたスキームを近似的に解くことにより，モデルに含まれる総ての物理過程を初期化過程に含めることができた。

寒冷前線が計算領域を通過中の事例についてDNIと規準モード初期化法（NMI）との比較を行ったところ，次のことが分った。（1）山脈による水平風のまわり込みやブロッキングはDNIの方がNMIより良く再現される。（2）DNIによる領域平均降水量の改善は大きくない。（3）予報初期3時間の降水量の平均2乗誤差はDNIにより明らかに改善される。

（*）現所属：気象研究所